Biomaterials Science

Accepted Manuscript

This article can be cited before page numbers have been issued, to do this please use: C. Kong, M. Hao, X. Chen, X. Zhao, Y. Wang, J. Li, Y. Gao, H. Zhang, B. Yang and J. Jiang, *Biomater. Sci.*, 2019, DOI: 10.1039/C8BM01007B.

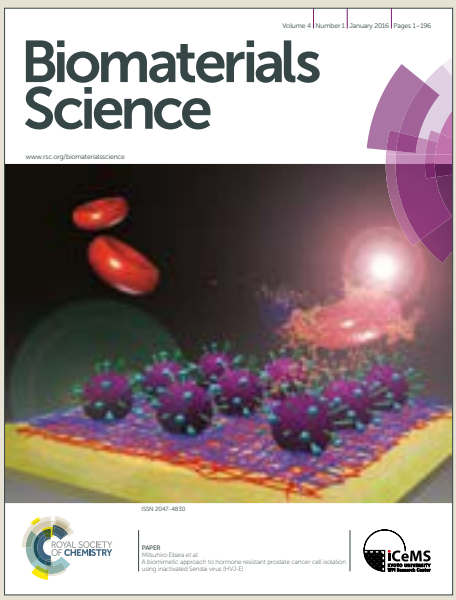

ROYAL SOCIETY OF CHEMISTRY

rsc.li/biomaterials-science

View Article Online
DOI: 10.1039/C8BM01007B

NF-κB Inhibition Promotes Apoptosis in Androgen-independent Prostate Cancer Cells by the Photothermal Effect via the IκBα/AR Signaling Pathway

Chenfei Kong[1#], Miao Hao[1#], Xi Chen[2], Xiaoming Zhao[1], Yuqian Wang[1], Jing Li[1], Yiyao Gao[1], Hao Zhang[3], Bai Yang[3], Jinlan Jiang[1*]

[1] Scientific Research Center, [2] Department of Anesthesiology, China-Japan Union Hospital of Jilin University, Changchun 130033, China

[3] State Key Laboratory of Supramolecular Structure and Materials, College of Chemistry of Jilin University, Changchun 130012, China

# These authors contributed equally to this work.

*Correspondence: Jinlan Jiang. Scientific Research Center, China-Japan Union Hospital of Jilin University, 126 Xiantai Street, Changchun, 130033, China

Tel: +86 431 8499 5443; Email: jiangjinlan@jlu.edu.cn

Abstract

The photothermal response of nanomaterials provides a basis for many biomedical applications, including diagnosis (e.g., biosensor and photoacoustic imaging) and treatment (e.g., drug delivery and photothermal therapy). The use of nano-materials for cancer phototherapy (solid tumor ablation) can cause cell necrosis and apoptosis. However, photothermal effects using the same material can differ among tumor cell types, and the molecular mechanisms underlying these differences are not clear. We used polydopamine (PDA)-coated branched Au−Ag nanoparticles (Au-Ag@PDA NPs) for the photothermal treatment of two prostate cancer cell lines. The therapeutic

View Article Online
DOI: 10.1039/C8BM01007B

effect was evaluated by CCK8, flow cytometry, and expression analyses of related genes by western blotting. Photothermal therapy resulted in oxidative stress in prostate cancer cells and activated the mitochondrial-related apoptosis pathway, increasing Bax expression. In addition, we observed a greater photothermal treatment effect on the androgen-dependent cells LNCaP than the androgen-independent cells DU145. Pretreatment with an inhibitor of NF-κB signaling pathway (BAY 11-7082) enhanced the expression of BAX in DU145 cells and increased the sensitivity of cells to the heat treatment of Au-Ag@PDA NPs both in vitro and in vivo. Our findings explain differences in the observed effects of photothermal therapy and provide direction for further improvements to this strategy.

Keywords

prostate cancer, photothermal effect, NF-κB, nanoparticle, androgen, apoptosis

1. Introduction

Photothermal therapy is an alternative cancer treatment after surgery, radiotherapy, chemotherapy, and biological therapy[1, 2]. Nano-gold-mediated hyperthermia has recently received widespread attention. In brief, when near-infrared laser light effectively passes through the human body, the plasma near the surface of gold nanoparticles can undergo plasmon resonance. This results in the absorbance of light energy and eventually conversion to heat energy, which is effectively transferred to environmental cells to produce a heat-killing effect[3-5]. Tumor cells exhibit poor heat resistance and therefore can be killed by this method, suggesting therapeutic applications.

Prostate cancer is the second most common type of cancer and the fifth leading cause of cancer-related deaths in men[6]. In 2012, it occurred in 1.1 million men and caused 307,000 deaths[7]. It can be divided into androgen-independent or

androgen-dependent subtypes. Androgen and the androgen receptor (AR) play important roles in the development and maintenance of prostate cancer[8, 9]. Early prostate cancer is androgen-dependent, and most patients initially respond to endocrine therapy. However, after 14 to 30 months of treatment, patients gradually develop castration-resistant prostate cancer (CRPC), for which endocrine therapy is ineffective. The mechanism underlying the formation of CRPC is highly complex and has not been fully elucidated. It involves tumor heterogeneity, the amplification and mutation of androgen genes, changes in signal transduction pathways, and cancer stem cells[6-8]. Despite the gradual increase in CRPC drugs, clinical treatment remains a major challenge.

It has been confirmed that there is an interaction between inflammation and cancer progression, and more and more research is focused on this emerging field. Recent studies have shown that the nuclear factor (NF)-κB family of transcription factors plays an important role in the occurrence and progression of a variety of human malignancies, including prostate cancer[10]. NF-κB plays a key role in regulating apoptosis and can modulate the expression of various cell death control factors[11]. It is also important for the progression of human diseases by promoting inappropriate cell survival. Therefore, the use of small molecule inhibitors of NF-κB may provide novel therapeutic opportunities[12].

In the present study, we used polydopamine (PDA)-coated branched Au−Ag nanoparticles (Au-Ag@PDA NPs) for photothermal therapy (PTT) using two prostate cancer cell lines and found that the photothermal effect can result in oxidative stress in prostate cancer cells, activate the mitochondrial-related apoptosis pathway, and increase the expression of Bax. The effect of PTT was greater for the androgen-dependent cells LNCaP than for the androgen-independent cells DU145. Treatment with an inhibitor of NF-κB signaling pathway (BAY 11-7082) enhanced the expression of BAX in DU145 cells and increased the sensitivity of cells to the heat treatment of Au-Ag@PDA NPs both in vitro and in vivo.

2. Materials and Methods

2.1 Preparation of Au–Ag@PDA NPs

Au−Ag@PDA nanoparticles were obtained from Professor Zhang Hao (Fig.1A)[13] and prepared as previously described, and are shown in Figure 1A. First, Ag seeds were synthesized according to the citrate reduction approach. Second, branched Au–Ag NPs were prepared using sacrificial Ag seeds, HAuCl4 aqueous solution, and the reductant of hydroquinone under room temperature. Third, to synthesize Au–Ag@PDA NPs, Tris buffer was added into the as-prepared Au–Ag NPs solution to alter the solution pH to 8.5, followed by addition of a dopamine solution and incubation at room temperature for 3 hours. Finally, Au–Ag@PDA NPs were obtained by centrifugation and washing with deionized water.

2.2 Reagents

Dulbecco's modified Eagle's medium (11965-092), RPMI 1640 (11875-093), fetal bovine serum (10270-106) and penicillin/streptomycin (15140122) were purchased from Gibco. Complete Protease Inhibitor Cocktail Tablets were purchased from Roche. Phenylmethanesulfonyl fluoride (P7626) and propidium iodide (P4170) were purchased from Sigma. Anti-casepase-3 (14220s), anti-caspase-8 (4790s), anti-Bax (2774) polyclonal antibodies and anti-β-actin monoclonal antibody (3700) were purchased from CST. Anti-p21 antibody (10355) was purchased from Proteintech. IRDye 800CW goat anti-mouse/rabbit IgG (926-32211) was purchased from Li-COR. Cell Counting Kit (CK04-3000T) was purchased from Dojindo. MDV-3100 (SC0074), NAC (S0077), BAY 11-7082 (S1523) and ROS Assay Kit (S0033) were purchased from Beyotime Institute of Biotechnology. Cell apoptosis detective kit (KGA108) was purchased from Kaiji Biotechnology Co., Ltd (Nanjing, China). Anti-Ki-67 Nuclear Antigen Monoclonal Antibody (ZM-0167), anti-Caspase-3 (PR-0284) and anti-Bax (PM-0258) polyclonal antibodies were purchased from Beijing Zhongshan Jinqiao Biotechnology Co., Ltd.

2.2 Cell culture

Human prostate cancer cell lines (LNCaP and DU145) were obtained from ATCC. LNCaP cells were grown in 1640 medium supplemented with 10% FBS and DU145 cells were grown in DMEM medium supplemented with 10% FBS. All the cells were maintained in humidified 5% CO_2 incubator.

View Article Online
DOI: 10.1039/C8BM01007B

2.3 TEM

Ultrathin sections of cells were analyzed by transmission electron microscopy to determine the distribution of Au−Ag@PDA NPs in the cells. After the cells were cultured in the medium containing Au−Ag@PDA NPs for 24 h, the dishes were washed with PBS to remove excess unbound nanoparticles. Cells were harvested and fixed with 2.5% glutaraldehyde for 2 h. The immobilized cells were then washed three times with PBS and stained with osmium tetroxide for 1 h at room temperature. After dehydration with a gradient of alcohol, the resin was embedded and ultrathin sections were prepared. The interaction of Au−Ag@PDA NPs with cells was observed and analyzed by transmission electron microscopy.

2.4 FT-IR spectra

BSA was procured from Sigma-Aldrich, Bangalore, India with 99% purity. Au−Ag@PDA NPs (2.5 mM) was suspended in phosphate buffer and then sonicated to obtain a homogeneous suspension. BSA of concentration (10 mM) in phosphate buffer was used. A mixture of ratio 1:1 was mixed and incubated for 3h. The Fourier transform–infrared (FT-IR) spectroscopy of NPs was performed by using a Bruker Vertex 70 FT-IR spectrometer (Bruker, Karlsruhe, Germany) in the range from 400 to 4,000 cm^{-1}.

2.5 Solution photothermal experiment

1 ml of different concentrations of Au−Ag@PDA NPs and DMEM medium were added in 24-well plate and placed under a laser at 808 nm. Laser power density of 5W / cm^2, the laser spot diameter of 1cm, just to be able to fully illuminate the solution. The temperature of the solution in the culture plate was measured with a thermometer.

2.6 Cytotoxicity Assay

The in vitro cytotoxicity tests were evaluated in 96-well culture plates. The Au−Ag@PDA NPs were foremost diluted to specific concentration using DMEM medium with 10% FBS. Cells were seeded in 96-well plates at an initial density of 3 × 10^3 cells/well in 0.1 mL of growth medium and incubated for 24 h prior to the addition of Au−Ag@PDA NPs. After the cellular supernatant was discarded, the cells were incubated in 100 μL different concentrations of Au−Ag@PDA NPs at 37 °C for

24 h. Cell Counting Kit (CCK8) assay was used to analyze the cell viability. The Au−Ag@PDA NPs in each concentration were assayed in three wells, and the assay was repeated three times. Cell viability was determined using the equation below.

Cell viability (%) =A(Treatment group)/B(Control group)×100%

2.7 Apoptosis and Necrosis Staining

The cells were seeded at 1.0 × 10^5cells/well in a 24-well flat-bottomed tissue culture plate and incubated for 24 h. After the cellular supernatant was discarded, the cells were incubated in 1 mL of culture medium with different concentration of Au−Ag@PDA NPs for 24 h. The samples were irradiated by an 808 nm NIR laser with 5W for 4 min. The cells were cultured for 2 h and stained with 0.05 mg/mL PI and Hoechst.

2.8 Intracellular reactive oxygen species (ROS) assay

Exactly 2 mL of cell suspension with cell concentration of 1×10^5 cells/mL was seeded per well in 6-well plates. The experimental grouping was the same as that in the section on CCK-8. After 24 h of incubation, the supernatant was aspirated, and the cells were washed twice with PBS and digested with 0.25% trypsin. Afterward, DMEM supplemented with 10% FBS was added to terminate digestion. The cells were suspended by pipetting, followed by centrifugation (1,000 rpm, 5 min). The supernatant was aspirated, and the cells were washed once with PBS and centrifuged again to obtain a cell pellet. The cells were stained with 200 μL of DCFH-DA (Shanghai Beyotime Bio-Tech Co., Ltd.) and incubated at 37°C for 20 min under the dark. The cells were then centrifuged, and the supernatant was removed. The cells were washed once with 500 μL of serum-free medium, followed by centrifugation (1,000 rpm, 5 min). The supernatant was aspirated, added with 200 μL of serum-free medium, and thoroughly mixed. Subsequently, the cells were detected via flow cytometry (FACS Aria; BD Corporation, San Jose, CA, USA). In some experiments, cells were pretreated with 5 mM NAC for 2 h prior exposure to compounds and analysis of ROS generation.

2.9 Quantitative analysis of apoptosis rate by Annexin V-FITC/PI double-staining assay

Cell density and experimental grouping were similar to those in the section on intracellular ROS assay. The supernatant was aspirated after incubation for 24 h, and the cells were washed twice with PBS and digested with 0.25% trypsin. DMEM supplemented with 10% FBS was then added to terminate digestion. The cells were suspended by pipetting, followed by centrifugation (1,000 rpm, 5 min). The supernatant was aspirated, and the cells were washed once with PBS and centrifuged again to obtain a cell pellet. Exactly 200 μL of binding buffer was added and mixed thoroughly. The cells were stained with 5 μL of Annexin V-FITC (Becton Dickinson Bioscience Company) and incubated in the dark at room temperature for 10 min. The cells were then centrifuged, and the supernatant was removed. Exactly 200 μL of binding buffer was added and mixed thoroughly. Subsequently, 5 μL of propidium iodide (PI) was added to stain the cells. After treatment, the cells were detected by flow cytometry.

2.10 Western blot analysis

Cell monolayers were washed twice with PBS, harvested, and lysed with ice-cold radioimmunoprecipitation assay buffer (Sigma-Aldrich) after which protein lysates (20 micrograms) were subjected to SDS- PAGE and Western blotting. The antibodies used for immunoblotting included those raised against caspase-3 (14220s), Caspase-8, (4790s), BAX (5023), IκBα, Phospho-IκBα (4812/2859; Cell Signaling Technology), AR and GAPDH (loading control; Sigma-Aldrich), p21 (10355; Proteintech). Antibody binding was detected by Infrared Imaging System (Odyssey).

2.11 Immunofluorescent staining and imaging

Cells were grown in a 96-well plate and washed three times with PBS then fixed in 4% formaldehyde solution and permeabilized with 0.1% Triton X-100 in PBS for 5 min. Cells were blocked with 2% BSA in PBS for 30 min at room temperature. Cells were incubated with respective Anti-p21 primary antibodies at 1：100 dilutions for 1 hr and then washed with PBS and incubated for 1 hr with TRITC-conjugated secondary antibodies at 1 ： 50 dilutions (Zhongshan, China). Cells were further washed in PBS and mounted with Vectashield mounting medium containing 4′ , 6-diamidino-2-phenylindole (DAPI; Vector Laboratories). The plates were scanned,

View Article Online
DOI: 10.1039/C8BM01007B

and images collected with an Operetta HTS imaging system (PerkinElmer).

2.12 Animal and tumor model

Male BALB/c athymic nude mice, 6-8 weeks of age and weighting 18-22 g were purchased from Shanghai LAC Laboratory Animal Co. Ltd., and housed in a SPF grade animal center. The use of all mice in this study complied with the current ethical considerations: Approval of institutional Animal Care and Use Committee of Jilin University. The mice were anesthetized by isoflurane, and 1×10^7 cells suspended in 100μL saline were transplanted subcutaneously into the mice. And then all the mice were housed in animal center until the tumor size reached ≈ 150 mm3. All animal procedures were performed in accordance with the Guidelines for Care and Use of Laboratory Animals of Jilin University and approved by the Animal Ethics Committee of Jilin University.

2.13 In vivo photothermal therapy

For photothermal therapy, when the tumors grew to 5–6 mm in diameter, the mice were randomly divided into three groups (n=6 per group), namely control, Au−Ag@PDA NPs and Au−Ag@PDA NPs+BAY. Mice of each group were intravenously subcutaneous injected with 100 μL of PBS, Au−Ag@PDA NPs, or Au−Ag@PDA NPs+BAY. The mice were anesthetized with chloral hydrate (5%), and the tumors were irradiated with an 808 nm laser (1.0 W/cm^2) for 4 min after 2 h injection. After treatments, the length and width of the tumors were tracked with a caliper every 2 days for 30 days. The tumor volume was calculated as follows: Tumor volume = (tumor length) × (tumor width) ^{2}/2.

2.14 Histological analysis

BALB/c mice from the treatment group were killed, and the tumor tissues and other major organs including heart, liver, spleen, lung, and kidney were collected for analysis after various treatments. The frozen tissue slides were further stained with hematoxylin and eosin following the standard protocol and examined using a fluorescence microscope.

2.15 Statistical analysis

All the results are expressed as the mean ± standard deviation (SD). Statistical

differences between the groups were determined using the Student's t-test and a $p < 0.05$ was considered statistically significant.

3 Results

3.1 Branched Au−Ag@PDA NPs are highly efficient photothermal agents

A schematic illustration of the synthesis of Au–Ag@PDA NPs, based on the previously reported method, is shown in Figure 1A. Our previous studies have shown that Au-Ag@PDA NPs have photothermal applications. In order to explore the possibility of Au-Ag@PDA NPs application in vivo, we studied the interaction of Au-Ag@PDA NPs with bovine serum albumin in vitro. Infrared spectroscopy showed that there were N-H stretching absorption bands in BSA + Au-Ag@PDA NPs and BSA groups at 3064 cm^{-1}, but not in Au-Ag@PDA NPs group (Figure 1B). These results suggested that there are interactions between Au−Ag@PDA and BSA.

Next, we analyzed the intracellular distribution of Au-Ag@PDA NPs. In particular, we used inverted microscopy and transmission electron microscopy to examine Au-Ag@PDA NPs-treated DU145 and LNCaP cells. As shown in Figure 1C, after 24 hours of co-culture with cells, many vacuoles formed inside the cell membrane and a large number of nanoparticles aggregated. The nanoparticles were clustered within cells. The nanoparticles can enter DU145 and LNCaP cells by endocytosis and accumulate in lysosomes. Based on magnified images, nanoparticles dispersed alone can still be observed in these nanoparticle clusters.

To further study their application to tumor PTT and the molecular mechanisms underlying their effects, we evaluated the toxicity of Au-Ag@PDA NPs against normal 293T human embryonic kidney cells. A CCK8 assay showed that the survival rate of 293T cells was greater than 90% when the concentration of Au-Ag@PDA NPs was less than 200μg/mL (Fig.1D). This suggests that Au-Ag@PDA NPs are not cytotoxic toward normal cells.

In an analysis of photothermal properties, solutions with various concentration gradients were added and irradiated with an 808-nm laser at 5 W/cm^2 for various time periods. The temperature change of the solution was recorded. As shown in Figure 2A, after laser irradiation for 4 min, the temperature of the solution tended to stabilize. As

the solution concentration increased, the temperature of the solution increased with increasing temperature, demonstrating a strong photothermal effect.

Next, we evaluated the killing effect of Au-Ag@PDA NPs on prostate cancer cells in vitro. DU145 and LNCaP cells were seeded on 96-well plates and incubated with Au-Ag@PDA NPs for 24 h followed by 808-nm NIR laser irradiation. Cell activity was measured by CCK8 assays after 2 h of light exposure. The results showed that in the absence of NPs, the laser irradiation had no effect on the cell activity (Fig.2B). In view of the low toxicity of the nanoparticles, we chose 0, 20, 40 and 80 ug/mL concentration of Au-Ag@PDA NPs to detect its photothermal effects. After laser treatment, high concentrations of Au-Ag@PDA NPs had significant effects on both LNCaP cells and DU145 cells. After irradiation with an 808-nm laser, 80 μg/mL Au-Ag@PDA NPs can cause approximately 80% prostate cancer cell death (Fig.2C).

3.2 Photothermal therapy has different effects on androgen-dependent and androgen-independent prostate cancer cells

Using CCK8 experiments, we further found that Au-Ag@PDA NPs PTT has different killing effects on different prostate cancer cell types (Fig.2C). The effect of Au-Ag@PDA NPs on LNCaP cells was substantial. Cell viabilities were 57%, 35%, and 15% in the presence of 20μg/mL, 40μg/mL, and 80μg/mL Au-Ag@PDA NPs, respectively. In DU145 cells, only 80 μg/mL Au-Ag@PDA NPs had a good photothermal effect.

We further confirmed the observed effects by immunofluorescence staining and flow cytometry. The staining results showed that 80 μg/mL nanomaterials could induce a large number of necrotic DU145 cells, while obvious necrosis in LNCaP cells could be seen in response to 40 μg/mL Au-Ag@PDA NPs irradiation (Fig.3E). Similar results were obtained by flow cytometry. Annexin V-FITC/PI double staining can be used to quantitatively detect apoptosis. As shown in Figure 3B-E, 40 μg/mL Au-Ag@PDA NPs can induce apoptosis and necrosis in about 23% DU145 cells. But in LNCAP cells, the apoptotic and necrotic rates were about 46% under the same conditions.

Next, we investigated changes in the expression of apoptosis-related proteins. Caspases are members of the endoproteinase family and play key roles in the regulation of cellular regulatory networks such as inflammation and cell death. Caspase-3, -6, -7, -8, and -9 are mainly involved in mammalian apoptosis. Accordingly, we analyzed changes in the expression of these molecules after PTT. As shown in Figure 3F, the expression levels of pro-caspase-3 and -8 decreased after Au-Ag@PDA NPs PTT. In contrast, the expression levels of cleaved caspase-3 and -8 obviously increased as the nanoparticle dose increased in both DU145 and LNCaP cells. BAX is the most important pro-apoptotic protein in the Bcl-2 family[14, 15]. We found that BAX expression increased significantly after Au-Ag@PDA NPs PTT. Futhermore, we explored the expression of p21. Westernblot and immunofluorescence showed that p21 expression of was increased after Au-Ag@PDA NPs PTT.

These results demonstrated that different prostate cancer cells exhibit different responses to PTT using the same nanomaterials. Compared with the hormone-independent prostate cancer cells DU145, the hormone-dependent prostate cancer cells LNCaP were more sensitive to Au-Ag@PDA NPs PTT.

3.3 Au-Ag@PDA NPs PTT-induced apoptosis is dependent on intracellular ROS production in prostate cancer cells

ROS is produced by the reaction between the mitochondria and NADPH oxidase. Excessive ROS can cause inflammation, oxidative stress, and apoptosis. As shown in Figure 4, Au-Ag@PDA NPs caused prostate cancer cells to produce substantial ROS, indicating that Au-Ag@PDA NPs induce cell damage after irradiation. Furthermore, the thiol-antioxidant NAC inhibited the Au-Ag@PDA NPs PTT-induced ROS generation in both DU145 and LNCaP cells. These results suggested that Au-Ag@PDA NPs PTT-induced ROS production is a cause of prostate cancer cell death.

3.4 BAY 11-7082 promotes apoptosis in androgen-independent prostate cancer

View Article Online
DOI: 10.1039/C8BM01007B

cells by the photothermal effect

Numerous studies have shown that NF-κB has anti-apoptotic effects and is closely related to tumor cell resistance. Therefore, we applied BAY 11-7082 to inhibit IκBα phosphorylation and evaluated the photothermal efficacy of the Au-Ag@PDA NPs in cells[16-18]. As shown in Figure 5B, using CCK8 assays, we found that BAY did not significantly affect the survival rate of cells in the control group. After the addition of various concentrations of Au-Ag@PDA NPs, the photothermal effects on DU145 cells were significantly enhanced, and cell viability decreased significantly at 40μg/mL. Similar results were obtained by immunofluorescence staining (Fig.5C). Apoptosis and necrosis of DU145 cells after PTT increased significantly after BAY addition (Fig.5D–E). Further, we analyzed the expression levels of apoptosis-related molecules. As shown in Figure 5F, western blotting showed that the expression levels of cleaved caspase3 and caspase8 increased after BAY treatment in DU145 cells. The apoptotic protein BAX was also upregulated. Interestingly, with BAY 11-7082 pretreatment, after Au-Ag@PDA NPs PTT, the p21 expression was upregulated but significantly weaker than that of the untreated group. These results suggested that the production of p21 may also be regulated by the NF-κB signaling pathway.

3.5 BAY 11-7082 promotes apoptosis in androgen-independent prostate cancer cells in response to photothermal therapy via the IκBα/AR signaling pathway

We next evaluated the relationship between NF-κB and AR during photothermal therapy in prostate cancer. We first tested whether blocking the NF-κB pathway can affect the level of AR expression in DU145 cells. As shown in Figure 6A, the expression of AR in DU145 cells was significantly weaker than that in LNCaP cells. After blocking the NF-κB signaling pathway with BAY, the levels of AR in DU145 cells increased significantly (Fig. 6B).

Combined with our previous results showing that blocking the NF-κB pathway enhances photothermal efficacy, these results suggest that AR may be associated with PTT sensitivity in prostate cancer. Accordingly, we further analyzed the effect of AR on PTT in LNCaP cells. We blocked AR signaling using MDV3100 in LNCaP cells and evaluated apoptosis after PTT. Flow cytometry results showed that the apoptosis

rate of the MDV3100-treated group showed a significant decrease after PTT with 40 μg/mL Au-Ag@PDA NPs (Fig. 6D-E). Collectively, our results demonstrated that the NF-κB signaling pathway can affect the PTT sensitivity of prostate cancer by modulating the expression of AR.

3.6 In vivo photothermal therapy with Au−Ag@PDA NPs

Au-Ag@PDA NPs had a good phototoxic effect on tumor cells in vitro. We evaluated their effect on the treatment of subcutaneous tumors in vivo. DU145 cells were first xenografted onto the backs of mice. The tumor-bearing mice were randomly divided into three groups (control, Au-Ag@PDA NPs, and Au-Ag@PDA NPs + BAY groups) and were treated by the subcutaneous injection of materials when the tumor volume reached approximately 100 mm^3. The tumor volumes and body weights of mice in each group were monitored every other day for 30 days. As shown in Fig 7A, tumors in the control groups showed obvious growth. However, tumor growth was significantly inhibited in the Au-Ag@PDA NPs and Au-Ag@PDA NPs + BAY groups, and the tumor volumes were significantly reduced (Fig. 7B). To assess the systemic toxicity of the nanoparticles, we measured the body weight of all groups of mice during treatment and no significant weight loss was observed (Fig. 7C). In addition, we performed a pathological analysis of the main organs of mice after 30 days of treatment. HE staining showed no significant changes in heart, liver, spleen, lung, and kidney of mice (Fig. 7D). These results showed that Au-Ag@PDA NPs exert low systemic toxicity.

Further, we performed immunohistochemical analysis of tumor tissues in each group and found that tumors in the Au-Ag @ PDA NPs + BAY group showed severe necrosis after irradiation, as well as a high proportion of tumor cell structures and nuclei contraction. Tumors of the Au-Ag @ PDA NPs group also showed partial necrosis. In contrast, no significant necrosis was observed in the control group (Fig. 7E). These results are consistent with the trend in tumor growth. Similarly, an immunohistochemical analysis showed that caspase-3 and BAX levels were highest in tumors treated with Au-Ag @ PDA NPs and laser irradiation, indicating severe

apoptosis. The expression of tumor caspase-3 and BAX in the Au-Ag @ PDA NPs group was significantly higher than that in the control group, indicating that Au-Ag @ PD NPs PTT for prostate cancer has a good effect in vivo.

4 Discussion

Prostate cancer is common in men and accounts for approximately 6.6% of all cancer-related deaths[6]. Although androgen deprivation therapy remains the primary treatment for metastatic prostate cancer, most men eventually develop resistance to androgen deprivation therapy, leading to the development of CRPC [6, 9, 19]. At present, there is no effective treatment for CRPC in clinical practice. Therefore, the development of new chemical and biological treatments for CRPC is urgently needed[20]. PTT, a new method for treating tumors, has various advantages, including strong selectivity, non-invasiveness, and a wide application range, in addition it is a simple process which causes minimal damage to normal tissues[19]. It has shown great value in the fields of tumor therapy, drug release and control, and light-control implanted materials[3]. In this study, we used Au-Ag@PDA NPs to perform PTT on two types of prostate cancer cells. Au–Ag@PDA NPs represent a novel nanomaterial exhibiting better structural stability, biocompatibility, and higher photothermal transduction efficiency than conventional Au NPs, and also showed a more efficient inhibitory effect on the proliferation of HeLa cells, implying their potential value in cancer treatment[13]. Our previous studies also showed that Au-Ag@PDA NPs with appropriate laser irradiation, dramatically inhibited the proliferation bladder and colon cancer cells[21, 22]. In this study, we found higher chromatin condensation and apoptotic body formation, and enhanced protein expression of apoptosis- related markers (c-caspase 3, c-caspase 8, Bax, and p21,) following Au-Ag@PDA NPs treatment in the presence of NIR laser treatment clearly suggesing its superiority in effective chemo-photothermal therapy of resistant cancers. In vivo, Au-Ag@PDA NPs PTT also had an efficient therapeutic effect on prostate cancer xenografts.

Although PTT is a promising alternative to traditional cancer treatment, certain adverse irradiation conditions can lead to cell necrosis and cause harmful

pro-inflammatory responses that affect the therapeutic effect. Recent studies have shown that by regulating the conditions of PTT, cells can be controlled to undergo apoptosis rather than necrosis; this treatment strategy is very attractive because apoptosis prevents inflammatory responses from occurring. Researchers are exploring the intracellular signaling cascade activated by PTT. Apoptosis and necrosis are two mechanisms of PTT-induced cell death[23]. The most common cellular response to PTT in vitro is necrosis, although some studies have shown that apoptosis occurs under certain light conditions. The main mechanism depends on exposure conditions[24-26]. Specifically, high-energy irradiation can cause necrosis, while low-energy irradiation promotes apoptosis. As shown in Figure 3 and 4, we used Au-Ag@PDA NPs for PTT and found that PTT can cause oxidative stress in prostate cancer cells and activate the mitochondria-associated apoptosis pathway, increasing the expression of Bax. These results indicate that PTT can induce apoptosis in prostate cancer cells.

The exact mechanism underlying the development of hormone-refractory prostate cancer is not clear; researchers believe that chronic inflammation and abnormal proliferation of prostate epithelial cells play important roles[27]. NF-κB activates cellular processes that are essential for cell survival and proliferation and induces a strong inflammatory response by regulating downstream genes[6, 7].The constitutive activation of the classic NF-κB pathway is associated with a poor prognosis and is a key determinant of chemotherapy resistance[12, 28]. As shown in Figure 5, we used BAY 11-7082 to inhibit IκBα phosphorylation to block the NF-κB signaling pathway and found that it can promote apoptosis in androgen-independent prostate cancer cells in response to tumor nanophotothermal therapy. Consistent with previously published results that p21 expression may be regulated by NF-κB[29-31], with BAY 11-7082 pretreatment, the expression of p21 were upregulated but significantly weaker than the of the untreated group after Au-Ag@PDA NPs PTT. Cell cycle deregulation is one of the major hallmarks of cancer cells. The induction of cell cycle arrest may be an effective strategy to control the aberrant proliferation of cancer cells[32]. It has also been reported that p21 is a potent inhibitor of cyclin-dependent kinases capable of arresting cell cycle progression[33]. We also found that Au-Ag@PDA NPs PPT

decreased the protein levels of cyclin A, but increased the protein levels of p21 in T24 cells[22]. Thus, these results indicate that Au–Ag@PDA NPs PTT may modulate the expression of cell cycle-related proteins to induce S phase arrest and consequently inhibit the proliferation of cancer cells.

Furthermore, our results demonstrated that the NF-κB signaling pathway can affect the PTT sensitivity of prostate cancer by modulating AR expression. Several studies have revealed that AR and NF-κB signaling have a close relationship in the process of disease treatment. Consistent with our results, Koshimizu *et al.* demonstrated that NF-κB overexpression and decreased immunoexpression of AR in the muscular layer are related to structural damage and apoptosis in cimetidine-treated rat vas deferens[20]. Debelec-Butuner *et al.* reported the inflammation-mediated abrogation of androgen signaling in an in vitro model of prostate cell inflammation[21]. These studies indicated that the NF-κB signaling pathway can regulate the expression of AR and affect drug resistance in prostate cancer.

Successful anticancer therapy should effectively inhibit the proliferation of cancer cells in vivo. In fact, Au-Ag@PDA NPs significantly inhibited xenograft growth of prostate cancer cells in nude mice after PTT. The laser excitation intensity used for the xenograft model treatment is 1W/cm^2, which is different from their in vitro PTT ablation at the excitation intensity of 5 W/cm^2. Although some skin burns were also observed on the surface of the tumors in the treatment group, skin injuries healed spontaneously after about 7 days. More importantly, no toxicity was observed in the main organs of Au-Ag@PDA NPs PTT group, suggesting that the biocompatibility of Au-Ag@PDA NPs is suitable for in vivo photothermal treatment. In addition, we found that Au-Ag@PDA NPs could bind to BSA in vitro (Fig 1B). Therefore, we will further study the binding of Au-Ag@PDA NPs with proteins in vivo and its effects on inflammatory factors and C-reactive proteins.

In conclusion, we demonstrated that Au-Ag@PDA NPs PTT can cause oxidative stress in prostate cancer cells, activate the mitochondrial-related apoptosis pathway, and increase the expression of Bax. Furthermore, the PTT effect was greater in androgen-dependent LNCaP cells than in androgen-independent DU145 cells.

Pretreatment with an NF-κB signaling pathway inhibitor (BAY 11-7082) enhances the expression of BAX in DU145 cells and increases the sensitivity of cells to the heat treatment of Au-Ag@PDA NPs both in vitro and in vivo.

Conflicts of interest

The authors report no conflicts of interest in this work.

Acknowledgments

This work was supported by the National Natural Science Foundation of China (No. 81401966 and 81402395), Jilin Provincial Project (sczsy201614, sczsy201716, 2017F014, JJKH20180184KJ, JJKH20190074KJ, 20190103086JH), the research project of Bethune plan of Jilin University (No. 2015332, 2018B08).

References

1. P. Wust, B. Hildebrandt, G. Sreenivasa, B. Rau, J. Gellermann, H. Riess, R. Felix and P. M. Schlag, *Lancet Oncol*, 2002, **3**, 487-497.
2. R. Ben-Yosef, *Harefuah*, 2002, **141**, 418-421, 500.
3. A. Bucharskaya, G. Maslyakova, G. Terentyuk, A. Yakunin, Y. Avetisyan, O. Bibikova, E. Tuchina, B. Khlebtsov, N. Khlebtsov and V. Tuchin, *Int J Mol Sci*, 2016, **17**.
4. H. Daraee, A. Eatemadi, E. Abbasi, S. Fekri Aval, M. Kouhi and A. Akbarzadeh, *Artif Cells Nanomed Biotechnol*, 2016, **44**, 410-422.
5. V. Shanmugam, S. Selvakumar and C. S. Yeh, *Chem Soc Rev*, 2014, **43**, 6254-6287.
6. M. S. Cookson, W. T. Lowrance, M. H. Murad, A. S. Kibel and A. U. Association, *J Urol*, 2015, **193**, 491-499.
7. K. Ito, *Nat Rev Urol*, 2014, **11**, 197-212.
8. T. Hara, H. Miyazaki, A. Lee, C. P. Tran and R. E. Reiter, *Cancer Res*, 2008, **68**, 1128-1135.
9. Y. N. Wong, R. Ferraldeschi, G. Attard and J. de Bono, *Nat Rev Clin Oncol*, 2014, **11**, 365-376.
10. R. Jin, Y. Yi, F. E. Yull, T. S. Blackwell, P. E. Clark, T. Koyama, J. A. Smith and R. J. Matusik, *Cancer Res*, 2014, **74**, 2763-2772.
11. M. Karin, *Nature*, 2006, **441**, 431-436.
12. A. Garg and B. B. Aggarwal, *Leukemia*, 2002, **16**, 1053-1068.
13. J. Li, W. Wang, L. Zhao, L. Rong, S. Lan, H. Sun, H. Zhang and B. Yang, *ACS applied materials & interfaces*, 2015, **7**, 11613-11623.
14. B. Antonsson, *Cell Tissue Res*, 2001, **306**, 347-361.
15. J. M. Adams and S. Cory, *Oncogene*, 2007, **26**, 1324-1337.
16. C. Juliana, T. Fernandes-Alnemri, J. Wu, P. Datta, L. Solorzano, J. W. Yu, R. Meng, A. A. Quong, E. Latz, C. P. Scott and E. S. Alnemri, *J Biol Chem*, 2010, **285**, 9792-9802.
17. P. Kleniewska, A. Piechota-Polanczyk, L. Michalski, M. Michalska, E. Balcerczak, M. Zebrowska and A. Goraca, *Oxid Med Cell Longev*, 2013, **2013**, 308358.
18. R. L. Huang, Y. Yuan, G. M. Zou, G. Liu, J. Tu and Q. Li, *Stem Cells Dev*, 2014, **23**, 277-289.
19. T. Yasufuku, K. Shigemura, O. Matsumoto, S. Arakawa and M. Fujisawa, *J Infect Chemother*,

View Article Online
DOI: 10.1039/C8BM01007B

2010, **16**, 200-205.
20. J. J. Mohiuddin, B. R. Baker and R. C. Chen, *Nature reviews. Urology*, 2015, **12**, 145-154.
21. M. Hao, C. Kong, C. Jiang, R. Hou, X. Zhao, J. Li, Y. Wang, Y. Gao, H. Zhang, B. Yang and J. Jiang, *Acta biomaterialia*, 2019, **83**, 414-424.
22. X. Zhao, T. Qi, C. Kong, M. Hao, Y. Wang, J. Li, B. Liu, Y. Gao and J. Jiang, *International journal of nanomedicine*, 2018, **13**, 6413-6428.
23. S. J. Martin, C. M. Henry and S. P. Cullen, *Mol Cell*, 2012, **46**, 387-397.
24. T. Mocan, C. T. Matea, I. Cojocaru, I. Ilie, F. A. Tabaran, F. Zaharie, C. Iancu, D. Bartos and L. Mocan, *J Cancer*, 2014, **5**, 679-688.
25. X. Huang, B. Kang, W. Qian, M. A. Mackey, P. C. Chen, A. K. Oyelere, I. H. El-Sayed and M. A. El-Sayed, *J Biomed Opt*, 2010, **15**, 058002.
26. L. Tong and J. X. Cheng, *Nanomedicine (Lond)*, 2009, **4**, 265-276.
27. S. M. Crusz and F. R. Balkwill, *Nat Rev Clin Oncol*, 2015, **12**, 584-596.
28. C. Nakanishi and M. Toi, *Nat Rev Cancer*, 2005, **5**, 297-309.
29. C. S. Seitz, H. Deng, K. Hinata, Q. Lin and P. A. Khavari, *Cancer research*, 2000, **60**, 4085-4092.
30. D. Javelaud and F. Besancon, *Oncogene*, 2001, **20**, 4365-4372.
31. K. N. Pennington, J. A. Taylor, G. D. Bren and C. V. Paya, *Molecular and cellular biology*, 2001, **21**, 1930-1941.
32. B. Novak and J. J. Tyson, *Biochemical Society transactions*, 2003, **31**, 1526-1529.
33. K. Vermeulen, D. R. Van Bockstaele and Z. N. Berneman, *Cell proliferation*, 2003, **36**, 131-149.

Figure legends

Fig 1. Branched Au−Ag@PDA NPs are highly efficient photothermal agents.

A. PDA-coated branched Au−Ag (Au−Ag@PDA) NPs.

B. FT-IR spectra of Au-Ag@ PDA, BSA and Au-Ag@ PDA+BSA.

C. Binding of Au-Ag@ PDA NPs to prostate cancer cells and their distribution in cells, as determined by TEM.

D. Cytotoxicity of branched Au−Ag@PDA NPs. 293T cells were seeded in 100 μL of culture medium with various concentrations of Au−Ag@PDA NPs for 24 h and evaluated by CCK8 assays. $^{**}p < 0.01$.

Fig 2. Photothermal therapy of Au−Ag@PDA NPs in prostate cancer cells.

A. Light-to-heat conversion efficiency of Au−Ag@PDA NPs.

View Article Online
DOI: 10.1039/C8BM01007B

B. Cell viabilities of different groups. (Blank: no NPs + no laser; Au−Ag@PDA: 80 μg/mL NPs + no laser; laser irradiation: no NPs + laser; Au−Ag@PDA+ laser irradiation: 80 μg/mL NPs + laser). laser irradiation: 5 W/cm^2 for 4 minutes **$p < 0.01$.

C. Photothermal therapeutic effects of Au−Ag@PDA NPs in prostate cancer cells. DU145 and LNCaP cell viabilities after 808-nm laser irradiation with a power density of 5 W/cm^2 for 4 min. The cells were first incubated with various concentrations of branched Au−Ag@PDA NPs for 24 h. Each experiment was performed three times **$p < 0.01$.

Fig 3. Au-Ag@PDA NPs photothermal treatment elicits apoptosis in prostate cancer cells.

A. Immunofluorescence assays of cells treated with different concentrations of Au–Ag@PDA NPs after laser irradiation at 5 W/cm^2 for 4 minutes. Necrotic cells were strongly stained by PI (red); cell nuclei were labeled by Hoechst 33342 (blue). Each experiment was performed three times. Scale bar, 50 μm.

B–E. Apoptosis analysis of Au-Ag@PDA NPs-incubated cells after irradiation by the 808-nm laser. Cells were analyzed by flow cytometry followed by Annexin V-FITC/PI staining.

F. The anti-apoptotic and pro-apoptotic protein levels were analyzed by western blotting. GAPDH was used as a protein loading control.

Fig 4. Au-Ag@PDA NPs PTT-induced apoptosis relies on intracellular reactive oxygen species (ROS) production in prostate cancer cells. Intracellular ROS of DU145 (A-B) and LNCaP (C-D) cells were determined by the 2′,7′-dichlorofluorescein diacetate (DCFDA) assay using flow cytometry. Cells were pretreated with *N*-acetylcysteine (NAC; 5 mM for 2 h) before the addition of Au-Ag@PDA NPs. Intracellular ROS levels were determined by DCFDA assays using flow cytometry. All results are expressed as means ± S.E.M. (n = 3). *$p < 0.05$.

View Article Online
DOI: 10.1039/C8BM01007B

Fig 5. BAY 11-7082 promotes the apoptosis of androgen-independent prostate cancer cells in response to Au-Ag@PDA NPs PTT.

A. Inhibitory effect of BAY 11-7082. B. CCK8 assays of DU145 cells pretreated with or without BAY 11-7082. C. Immunofluorescence assays. Scale bar is 50 μm. D. Cell apoptosis analysis. Cells were analyzed by flow cytometry followed by Annexin V-FITC/PI staining. **p < 0.01. E. Intracellular ROS was determined by the DCFDA assay using flow cytometry. **p < 0.01. F. The anti-apoptotic and pro-apoptotic proteins were analyzed by western blotting. GAPDH was used as a protein loading control. G. Immunofluorescence assays of *p21* expression. Scale bar, 50 μm. **p < 0.01.

Fig 6. BAY 11-7082 promotes the apoptosis of DU145 cells by the photothermal effect via the IκBα/AR signaling pathway.

A. The mRNA expression level of *AR* was assessed by qPCR. **p < 0.01. B–C. The expression levels of AR in DU145 and LNCaP cells were assessed by western blotting. D-E. Cell apoptosis analysis of Au-Ag@PDA NPs-incubated LNCaP cells pretreated with or without MDV3100 (10μM) after irradiation by the 808-nm laser. **p < 0.01.

Fig 7. In vivo evaluation of the photothermal therapeutic effect.

A. Images of the tumors collected from different groups of mice. B. Tumor volumes for each group of mice. C. Body weight curves for each group of mice after treatment. D. Histological analysis of the major organs of mice after 30 days of treatment. E. Immunohistochemical assays of the tumor tissues of mice after treatment.

View Article Online
DOI: 10.1039/C8BM01007B

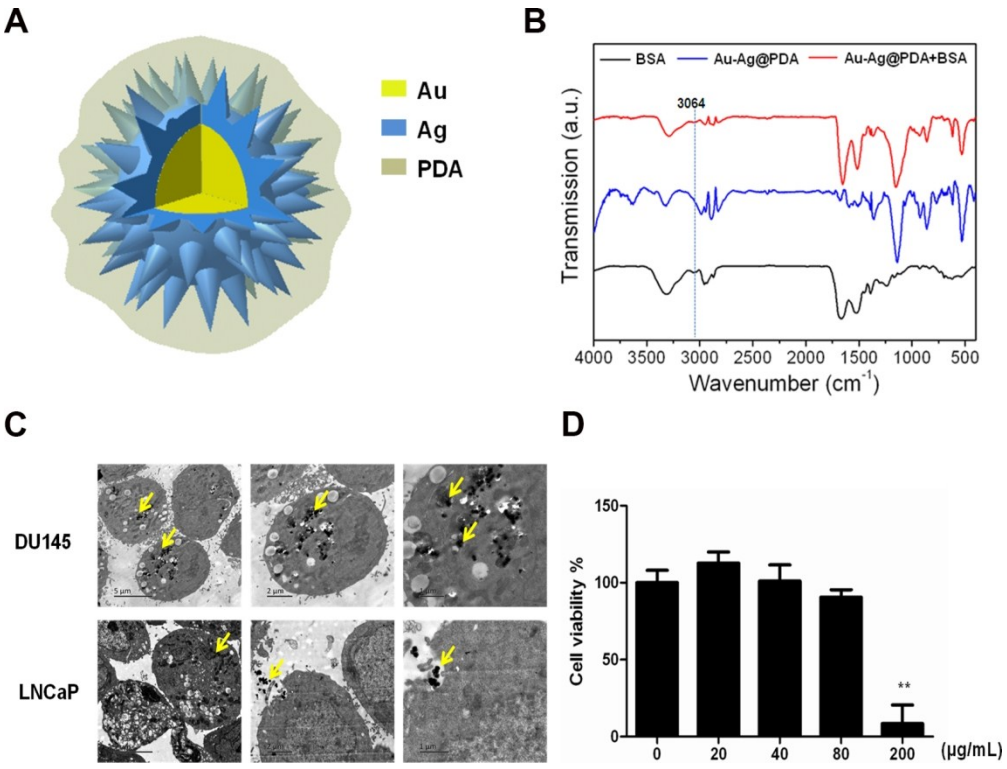

Fig 1. Branched Au−Ag@PDA NPs are highly efficient photothermal agents.

View Article Online
DOI: 10.1039/C8BM01007B

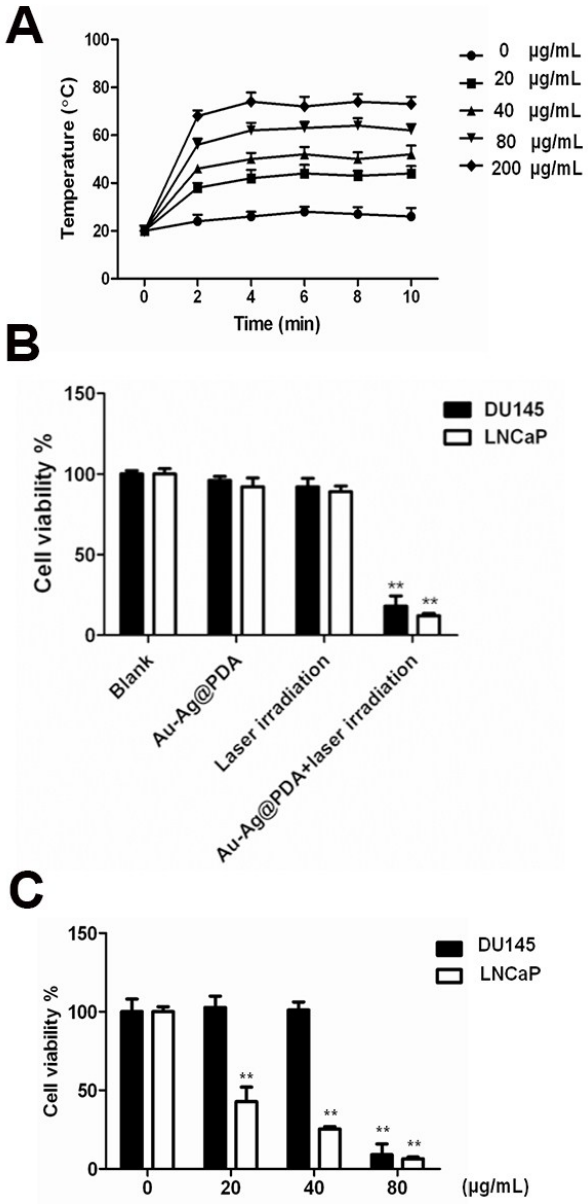

Fig 2. Photothermal therapy of Au−Ag@PDA NPs in prostate cancer cells.

View Article Online
DOI: 10.1039/C8BM01007B

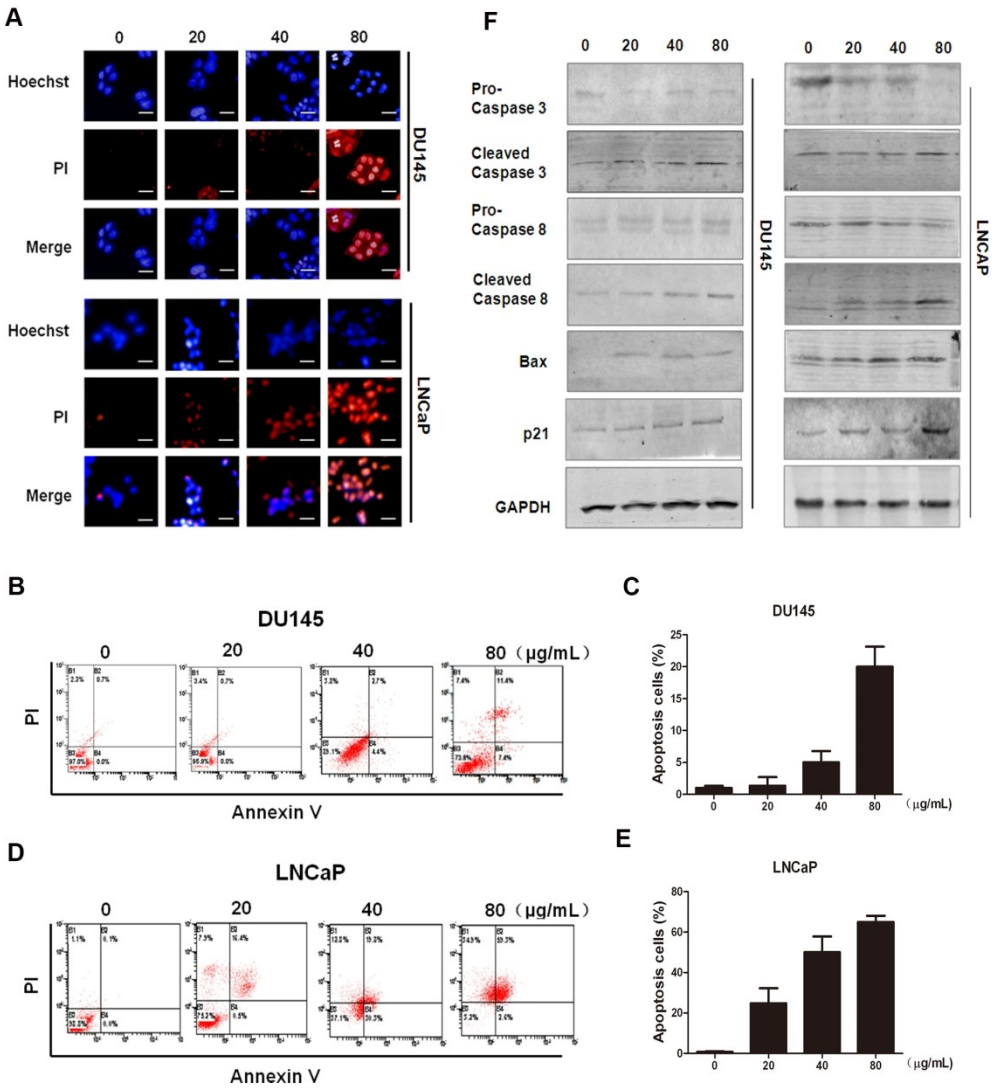

Fig 3. Au-Ag@PDA NPs photothermal treatment elicits apoptosis in prostate cancer cells.

View Article Online
DOI: 10.1039/C8BM01007B

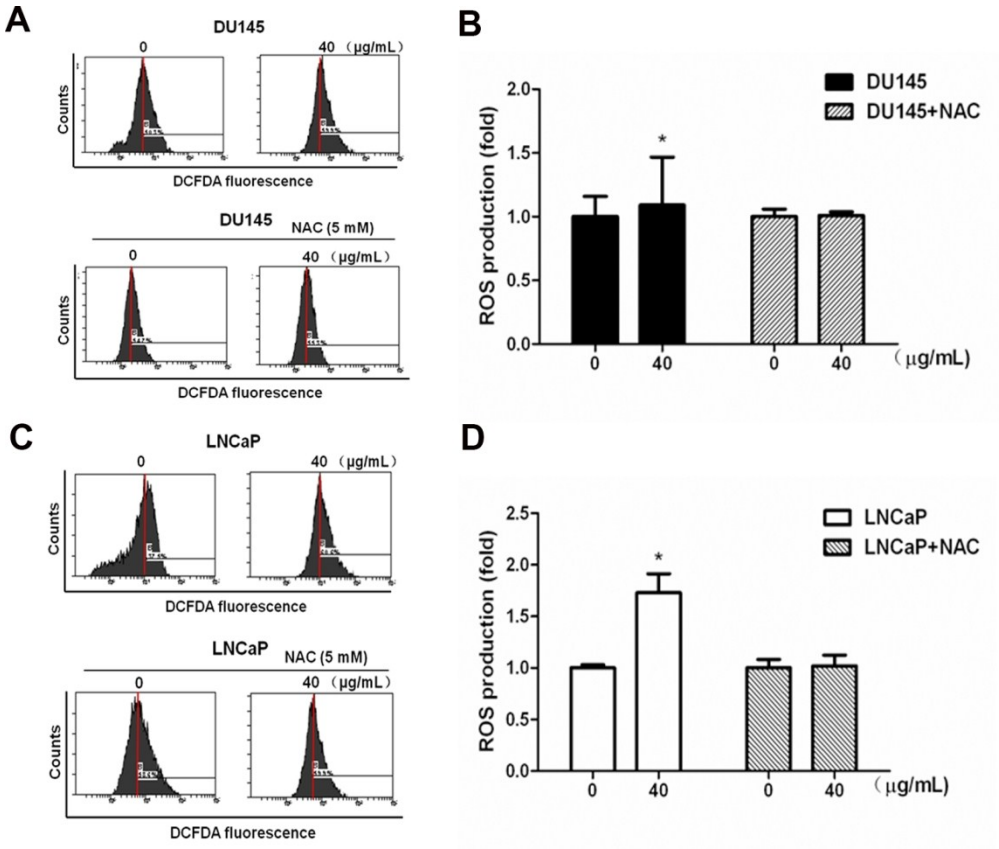

Fig 4. Au-Ag@PDA NPs PTT-induced apoptosis relies on intracellular reactive oxygen species (ROS) production in prostate cancer cells.

View Article Online
DOI: 10.1039/C8BM01007B

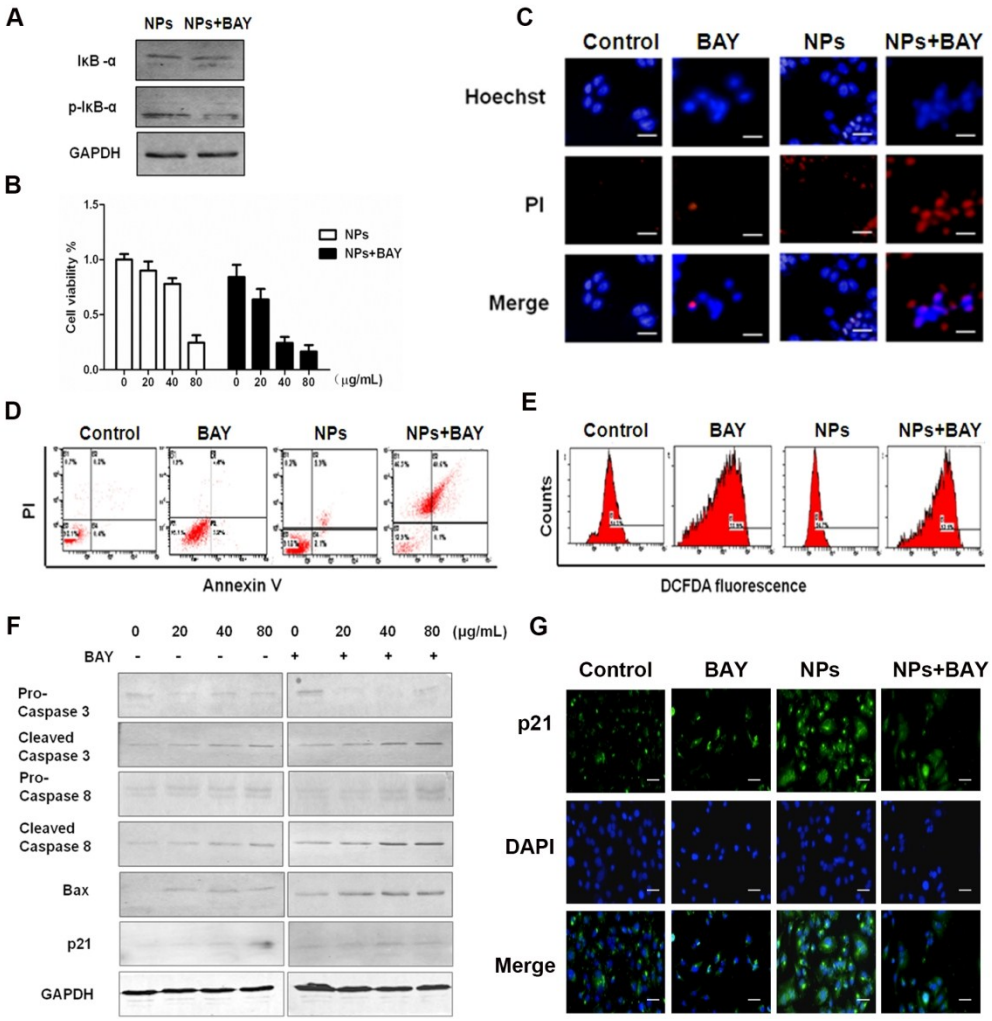

Fig 5. BAY 11-7082 promotes the apoptosis of androgen-independent prostate cancer cells in response to Au-Ag@PDA NPs PTT.

View Article Online
DOI: 10.1039/C8BM01007B

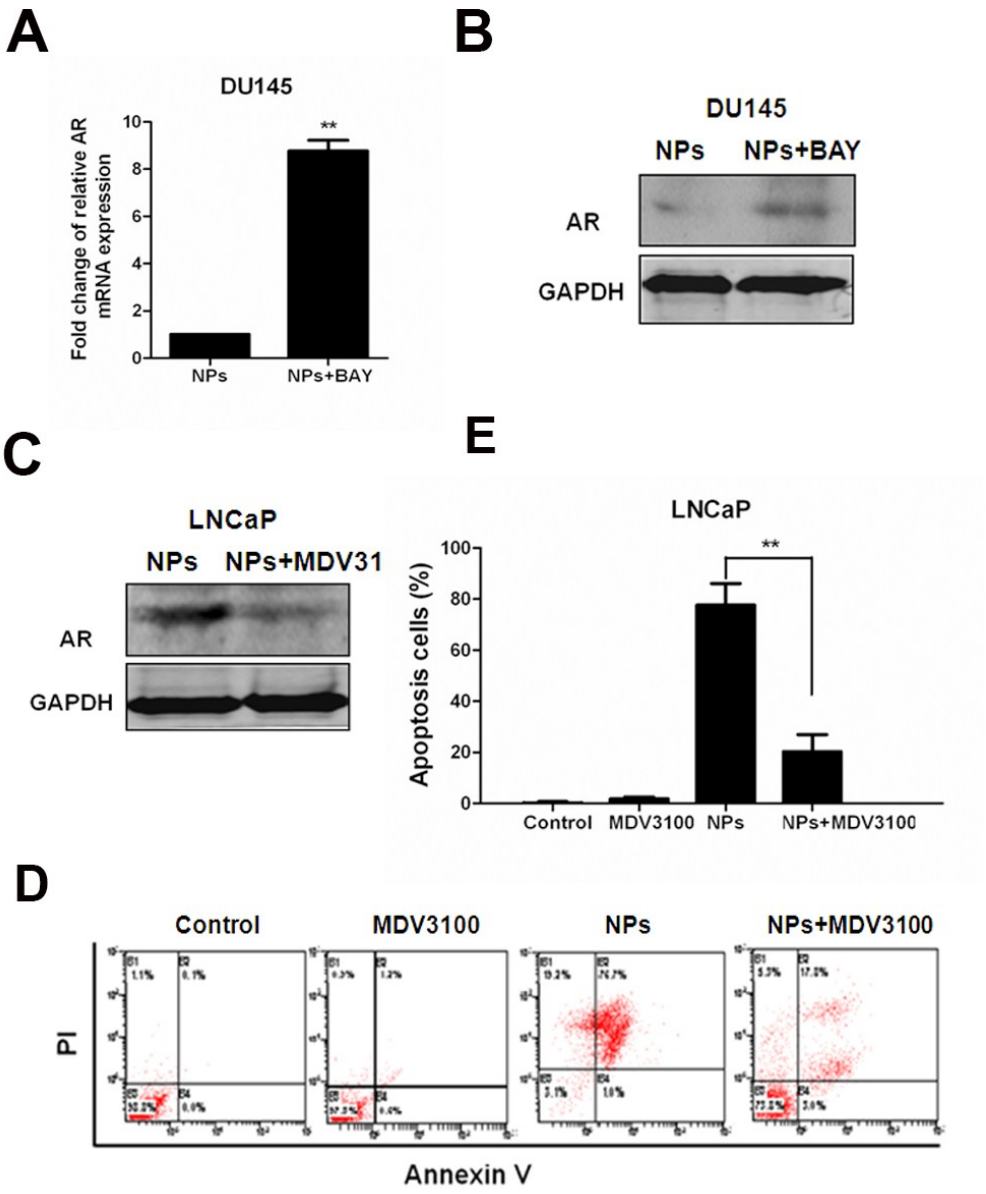

Fig 6. BAY 11-7082 promotes the apoptosis of DU145 cells by the photothermal effect via the IκBα/AR signaling pathway.

View Article Online
DOI: 10.1039/C8BM01007B

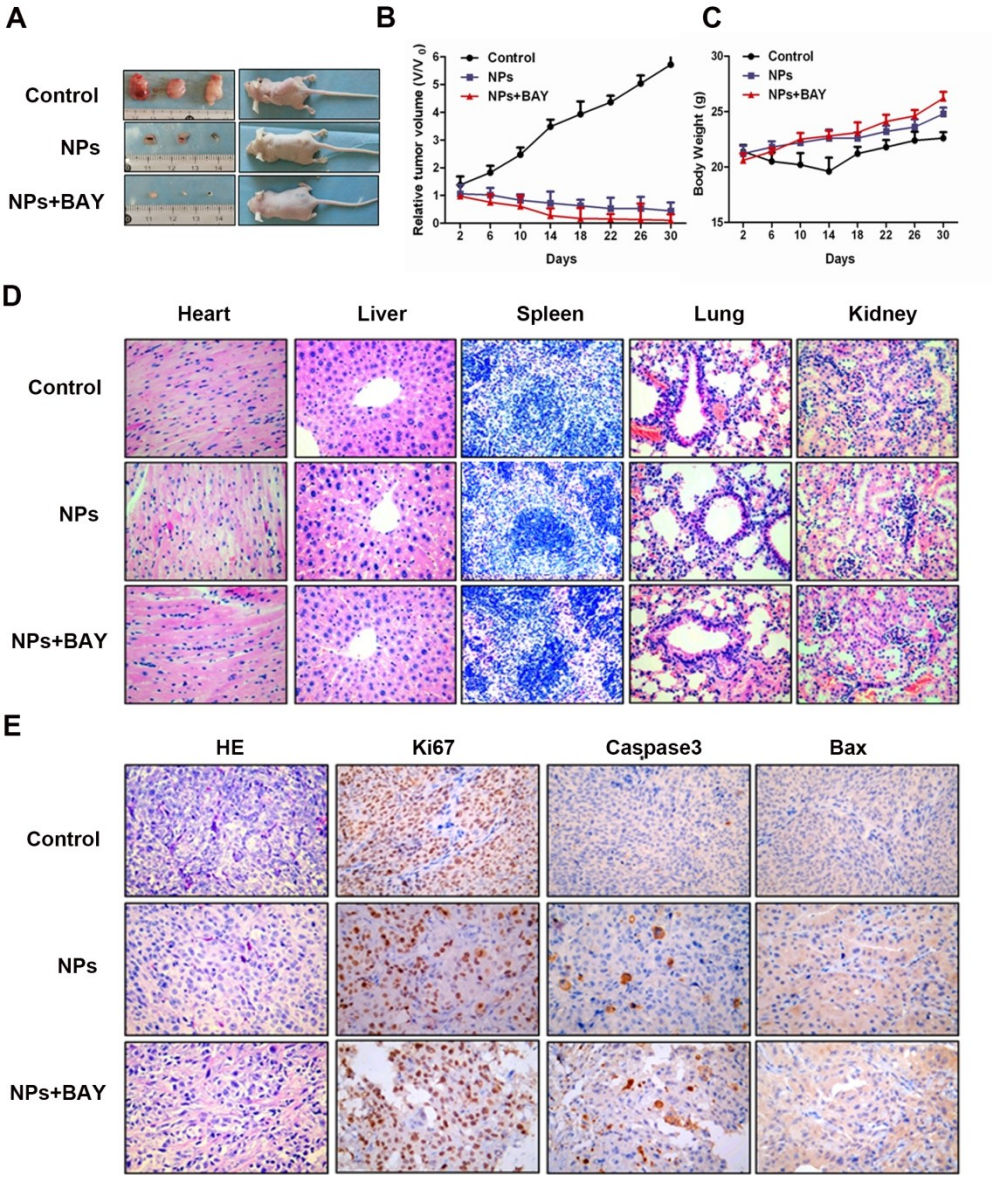

Fig 7. In vivo evaluation of the photothermal therapeutic effect.